Atmos. Meas. Tech. Discuss., 8, 3803–3850, 2015
www.atmos-meas-tech-discuss.net/8/3803/2015/
doi:10.5194/amtd-8-3803-2015

Atmospheric Measurement Techniques Discussions
Open Access

Detailed characterizations of a Comparative Reactivity Method (CRM) instrument: experiments vs. modelling

V. Michoud[1], R. F. Hansen[1,2,3,*], N. Locoge[1], P. S. Stevens[2,3], and S. Dusanter[1,2]

[1]Mines Douai, 59508, Douai, France
[2]School of Public and Environmental Affairs, Indiana University, Bloomington, IN, USA
[3]Department of chemistry, Indiana University, Bloomington, IN, USA
[*]now at: School of Chemistry, University of Leeds, Leeds, UK

Received: 1 April 2015 – Accepted: 2 April 2015 – Published: 16 April 2015

Correspondence to: S. Dusanter (sebastien.dusanter@mines-douai.fr) and V. Michoud (vincent.michoud@mines-douai.fr)

Published by Copernicus Publications on behalf of the European Geosciences Union.

Abstract

The Hydroxyl radical (OH) is an important oxidant in the daytime troposphere that controls the lifetime of most trace gases, whose oxidation leads to the formation of harmful secondary pollutants such as ozone (O_3) and Secondary Organic Aerosols (SOA). In spite of the importance of OH, uncertainties remain concerning its atmospheric budget and integrated measurements of the total sink of OH can help reducing these uncertainties. In this context, several methods have been developed to measure the first-order loss rate of ambient OH, called total OH reactivity. Among these techniques, the Comparative Reactivity Method (CRM) is promising and has already been widely used in the field and in atmospheric simulation chambers. This technique relies on monitoring competitive OH reactions between a reference molecule (pyrrole) and compounds present in ambient air inside a sampling reactor. However, artefacts and interferences exist for this method and a thorough characterization of the CRM technique is needed.

In this study, we present a detailed characterization of a CRM instrument, assessing the corrections that need to be applied on ambient measurements. The main corrections are, in the order of their integration in the data processing: (1) a correction for a change in relative humidity between zero air and ambient air, (2) a correction for the formation of spurious OH when artificially produced HO_2 react with NO in the sampling reactor, and (3) a correction for a deviation from pseudo first-order kinetics. The dependences of these artefacts to various measurable parameters, such as the pyrrole-to-OH ratio or the bimolecular reaction rate constants of ambient trace gases with OH are also studied. From these dependences, parameterizations are proposed to correct the OH reactivity measurements from the abovementioned artefacts.

A comparison of experimental and simulation results is then discussed. The simulations were performed using a 0-D box model including either (1) a simple chemical mechanism, taking into account the inorganic chemistry from IUPAC 2001 and a simple organic chemistry scheme including only a generic RO_2 compounds for all oxidized organic trace gases; and (2) a more exhaustive chemical mechanism, based on

AMTD
8, 3803–3850, 2015

the Master Chemical Mechanism (MCM), including the chemistry of the different trace gases used during laboratory experiments. Both mechanisms take into account self- and cross-reactions of radical species. The simulations using these mechanisms allow reproducing the magnitude of the corrections needed to account for NO interferences and a deviation from pseudo first-order kinetics, as well as their dependence on the Pyrrole-to-OH ratio and on bimolecular reaction rate constants of trace gases. The reasonable agreement found between laboratory experiments and model simulations gives confidence in the parameterizations proposed to correct the Total OH reactivity measured by CRM. However, it must be noted that the parameterizations presented in this paper are suitable for the CRM instrument used during the laboratory characterization and may be not appropriate for other CRM instruments, even if similar behaviours should be observed. It is therefore recommended that each group characterizes its own instrument following the recommendations given in this study.

Finally, the assessment of the limit of detection and total uncertainties is discussed and an example of field deployment of this CRM instrument is presented.

1 Introduction

The hydroxyl radical (OH) is known to be the main oxidant of the troposphere during daytime (Levy, 1972), leading to the oxidation of most atmospheric trace gases, including climate related compounds such as methane, and the formation of harmful secondary pollutants such as ozone (O_3) and Secondary Organic Aerosols (SOA). Due to the key role of OH in atmospheric chemistry, it is important to correctly describe the OH budget in atmospheric models. Field campaigns including OH measurements have been carried out to assess our understanding of the photochemical processes controlling the OH budget (see Stone et al., 2012, as a review). In these studies, measurements of OH concentrations are often compared to predictions from photochemical models that are constrained by measurements of long-lived species and environmental parameters (Carslaw et al., 2002; Martinez et al., 2003; Dusanter

AMTD
8, 3803–3850, 2015

et al., 2009; Hofzumahaus et al., 2009; Michoud et al., 2012). This approach allows testing our understanding of different aspects of the OH chemistry, i.e. sources, sinks and propagation reactions.

Volatile Organic Compounds (VOCs) are of particular interest for the OH chemistry since a large number of species (10^4–10^5), emitted by natural and anthropogenic sources, or formed photochemically, are expected to be present in the atmosphere (Goldstein and Galbally, 2007). However, measurements of VOCs are challenging and measuring an exhaustive suit of VOCs is unfeasible using current analytical techniques. During field campaigns, 60–70 VOCs are usually monitored, which is order of magnitudes lower than expected. Therefore, there are legitimate concerns regarding the completeness of the measured pool of VOCs and the use of these measurements to characterize the total sink of OH.

To address this issue, an integrated measurement of the total sink of OH, so called total OH reactivity, has been proposed by Calpani et al. (1999) and Kovacks et al. (2001). OH reactivity measurements are important for several reasons: (i) it allows to better constrain photochemical models during radical closure exercises, including the field campaigns mentioned previously, and consequently allows to focus on the representativeness of the chemical mechanism used, (ii) since OH is in steady state in the atmosphere due to its short lifetime, the measured total OH reactivity can be used together with measured OH concentrations to determine the total production rate of OH. The latter is compared to a production rate calculated from measured OH precursors, which provides a critical test of our understanding of OH sources (Whalley et al., 2011), (iii) finally, one can estimate the calculated OH reactivity using the measured trace gases to see whether unidentified reactive species are present in ambient air, with the goal of assessing their importance in terms of reactivity. If statistically significant, the difference observed between the measured and calculated values of OH reactivity is referred as the "missing OH reactivity".

Large missing OH reactivity is often found in different types of environments (Di Carlo et al., 2004; Lou et al., 2010; Dolgorouky et al., 2012; Hansen et al., 2014) highlighting

AMTD
8, 3803–3850, 2015

the presence of important unmeasured reactive compounds. This missing reactivity has been attributed to unidentified primary biogenic VOCs or unmeasured oxidation products of primary VOCs that has yet to be identified.

The first techniques proposed to measure total OH reactivity, the total OH loss rate method and the pump and probe method (Hansen et al., 2015), require the measurements of OH radicals using laser apparatus, making them costly and whose deployment requires highly skilled operators. More recently, a novel technique called Comparative Reactivity Method (CRM) has been developed to measure the total OH reactivity (Sinha et al., 2008). This technique does not need OH measurements and is based on monitoring the competition between a reference molecule (pyrrole) and compounds present in ambient air to react with artificially produced OH radicals inside a sampling reactor. The measurement of total OH reactivity is derived from a series of analytical steps during which the pyrrole concentration is quantified using a specific detector, being most of the time Proton Transfer Reaction-Mass Spectrometers (PTR-MS).

CRM instruments have been widely used during field campaigns (Sinha et al., 2008, 2010, 2012; Kim et al., 2011; Dolgorouky et al., 2012; Nölscher et al., 2012a, 2013; Hansen et al., 2015; Zannoni et al., 2015) or during chamber experiments in the laboratory (Nölscher et al., 2012b, 2014) since its development and new research groups are developing similar systems. Its deployment in the field led to important observations related to high missing reactivity during heat stressed conditions in a boreal forest (Nölscher et al., 2012a) due to unmeasured reactive VOCs from primary biogenic sources or oxidation products of biogenic compounds; as well as during the transport of aged continental air masses in an urban environment in Paris (Dolgorouky et al., 2012), likely due to unmeasured (multi-)oxidized compounds formed from the oxidation of anthropogenic emissions.

A new CRM instrument has been developed and coupled to a PTR-Time of Flight (ToF)-MS at Mines Douai (France) in 2012 and has been intercompared to the pump probe technique in a NO_x-rich environment (Hansen et al., 2015) and to another CRM instrument at a low-NO_x remote site (Zannoni et al., 2015). Generally, good agree-

AMTD
8, 3803–3850, 2015

ments and explanations for some deviations have been found between the CRM from Mines Douai and these two other instruments.

However, this technique requires multiple corrections (Hansen et al., 2015), especially to account for an interference to NO (Sinha et al., 2008; Dolgorouky et al., 2012), which limited its use to low NO_x environments, exception made of two studies (Dolgorouky et al., 2012; Hansen et al., 2015). Other corrections are also needed to derive reliable measurements of total OH reactivity due to (i) changes in humidity between the different steps of pyrrole measurements, (ii) deviations from pseudo first order kinetics which is assumed to derive OH reactivity measurements (Sinha et al., 2008), (iii) dilution of ambient air inside the reactor. While these corrections and interferences are known from the early use of CRM, a comprehensive characterization of the CRM technique as yet to be published.

In this study, we describe the CRM instrument constructed in Mines Douai (MD-CRM), highlighting the modifications brought in the setup since the first deployment of this instrument (Hansen et al., 2015). Then a detailed description of interferences and corrections needed to derive accurate OH reactivity measurements is presented based on intensive laboratory experiments. Furthermore, simulations of the chemical processes occurring inside the sampling reactor are compared to experimental observations made during the laboratory characterization. The simulations have been conducted using a simple mechanism of 42 reactions and using a more detailed mechanism: a subset of the Master Chemical Mechanism (MCM v3.2), including 1610 reactions. Finally, figures of merit such as limit of detection and measurement uncertainties are assessed.

AMTD
8, 3803–3850, 2015

2 The Comparative Reactivity Method (CRM)

2.1 General principle

The Comparative Reactivity Method relies on monitoring the competition between a reference molecule and trace gases present in ambient air to react with artificially produced OH radicals inside a sampling reactor. This technique has been first described in 2008 by Sinha et al. (2008) and has been discussed in details by Hansen et al. (2015). Briefly, a reference molecule that is not present in the atmosphere (pyrrole, C_4H_4NH), dry N_2, and dry zero air are first introduced into a reactor equipped with a UV pen ray Hg lamp. During this step, while the mercury lamp is ON, no OH is produced inside the reactor due to the dry conditions. The pyrrole concentration (C1) is monitored using a suitable detector, most of the time by PTR-MS at the protonated m/z 68. The C1 concentration corresponds to the initial amount of pyrrole inside the reactor after potential photolysis due to photons from the mercury lamp leaking inside the reactor. Then, dry zero air and dry N_2 are replaced by wet zero air and wet N_2 leading to the generation of OH radicals inside the reactor (due to H_2O photolysis). A decrease of the pyrrole concentration (C2) is observed due to reaction of pyrrole with the generated OH. Once the C2 concentration is acquired, wet zero air is replaced by ambient air and a competition occurs for OH between pyrrole and ambient reactive compounds. This competition leads to an increase of the pyrrole concentration to C3. A schematic of the pyrrole levels observed during these three measurement steps is shown in Fig. 1 (inserted graphic). The OH reactivity is then calculated using Eq. (1), assuming first order kinetics, with k_p corresponding to the kinetic rate constant of the reaction between pyrrole and OH (1.2×10^{-10} cm^3 molecules^{-1} s^{-1} at 25 °C (Atkinson et al., 1984; Dillon et al., 2012)).

$$k_{OH} = \frac{(C3 - C2)}{(C1 - C3)} \cdot k_p \cdot C1 \quad (1)$$

AMTD
8, 3803–3850, 2015

As the method described above to get the C1 concentration (dry method) takes a long time, e.g. 2–3 h, since completely dry conditions are needed inside the reactor, and tends to overestimate the photolysis of pyrrole inside the reactor due to residual water, the scavenger method (Zannoni et al., 2015) has been used for our system. As described in Zannoni et al. (2015), this new method consists in introducing an elevated concentration of a specific species (here propane at approximately 900 ppm) acting as a scavenger for the OH radicals. This approach is advantageous since it takes only a few minutes and it can be applied keeping the wet conditions needed for the other steps of the measurements.

As stated in the introduction, this technic suffers from several measurement artefacts or interferences for which the measured values need to be corrected. Corrections, in the order of their application in the data processing, are:

- correction on C2 for variations of RH between C2 and C3;
- correction on C3 for the spurious OH production from the reaction between HO_2 (formed from H_2O photolysis) and NO;
- correction on reactivity values calculated from Eq. (1) for a deviation from pseudo first order kinetics;
- correction on reactivity values for dilution, due to the N_2 flow introduced in the reactor.

2.2 Setup of the CRM instrument developed at Mines Douai (MD-CRM)

A description of the CRM instrument developed at Mines Douai (MD-CRM) as well as its operating conditions are given in this section. The MD-CRM instrument has been previously described in Hansen et al. (2015) and a schematic is shown in Fig. 1. Several improvements have been performed since its first deployment during the intercomparison exercise presented in Hansen et al. (2015), in particular to lower pyrrole photolysis below 5 % by changing the UV pen ray Hg lamp position in the setup (Laser

AMTD
8, 3803–3850, 2015

Components, model 11SC-1). As a consequence, the photolysis of other trace gases in the reactor has also been reduced. As discussed in Hansen et al. (2015), photolysis of VOCs into the CRM reactor led to unaccounted OH reactivity during tests performed using synthetic VOC mixtures. Up to 55 % of the OH reactivity was not measured for a complex OVOC mixture. For the current MD-CRM setup, direct observations of VOC photolysis inside the reactor indicate less than 1 % of photolysis for OVOCs such as methanol, acetaldehyde, acetone, methylethylketone... In contrast to what was observed with the prior version of this instrument, the new setup allows reconciling measured and calculated reactivity within 9 % for similar VOC mixtures (see Supplement Sect. S1).

Pyrrole (Praxair, 10 ppm in N_2) and N_2 (Air Liquide, alpha gaz 2; or Praxair, N_2 6.0) are introduced in a glass flow reactor built by the Max Planck Institut für Chemie (Mainz, Germany) at flow rates of 2.3 and 70 mL min^{-1}, respectively. N_2 was humidified by passing it through a bubbler or was kept dry, depending on the measurement step. The C1-C2-C3 pyrrole mixing ratios were monitored by a PTR-ToFMS instrument (Kore Technology, second generation), whose sampling flow rate was kept constant at 145 mL min^{-1} using a mass flow controller (MFC) (MKS inst, 200 sccm). Dry zero air was produced by an air generator including a compressor (CLAIND, model 2301TOC). For wet conditions, humid zero air was generated by sampling ambient air through a catalytic converter (stainless steel tubing filled with Pt wool held at 350 °C) in order to generate zero air at the same relative humidity (RH) than ambient air (prior 2014). More recently (after 2014), the humid zero air was generated using a similar air generator than for the dry conditions. The flow of dry air is split and passes through two MFCs (MKS inst., 500 sccm), one of them being sent through a water bubbler. The two flows are then mixed together to generate wet zero air at a specific RH. Two RH probes (Measurements Specialties Inc, model HM1500LF) are mounted in this set up for measuring RH in both the generated humidified air and in ambient air. The flows of the two MFCs (Dry and Humid zero air) are controlled using a LabView (National instrument) program to get the same RH in zero and ambient air. This new setup has

AMTD
8, 3803–3850, 2015

been designed for high NO_x environments since these species are not suppressed from ambient air using a catalytic converter, which in turn can lead to erroneous measurements of C2. Finally, a pump draws 240 mL min^{-1} at the end of the reactor. In this configuration, approximately 310 mL min^{-1} of zero air (during C1 and C2) or of ambient air (during C3) is sampled by the CRM instrument.

To minimize the residence time inside the sampling line, a Teflon pump is added upstream of the reactor sampling ambient air at approximately 1 L min^{-1}, with the extra air going to an exhaust. This pump is only installed during field campaigns and all the laboratory tests presented in this study have been conducted without it.

2.3 Description of experiments conducted to assess the CRM corrections

For the laboratory tests presented in this study, the CRM is usually kept under C2 conditions (humid zero air provided to the reactor) and standards of different natures (VOCs or NO_x) are directly injected in the line bringing zero air to the reactor as shown in Fig. 1. The description of the tests presented in this study is given in this section.

2.3.1 Changes in RH between C2 and C3

While the use of a catalytic converter reduced differences in RH between C2 and C3, small differences are still observed. Since the concentration of OH inside the reactor is driven by photolysis of water, a small difference can lead to significant different OH levels between C2 and C3, and as a consequence to an artefact in the C2 measurement (Sinha et al., 2008). Therefore, a correction is directly applied on the pyrrole concentrations measured during C2. To assess this correction, experimental determinations of the C2 sensitivity to humidity are performed measuring C2 at various RH before, during, and after field campaigns, by introducing various flows (from 50 to 300 sccm) of dry zero air inside the sampling line. The dilution of humid ambient air with dry zero air allows to change RH on a large range (typically 20–60 %, Fig. 2).

AMTD
8, 3803–3850, 2015

To track the relative humidity during these experiments and during ambient measurements of OH reactivity, we use the ratio between m/z 37 (cluster ion $H_3O^+.H_2O$) and m/z 19 (H_3O^+) monitored by PTR-ToFMS. Indeed, H_3O^+ ions can cluster in the drift tube of the PTR-MS (DeGouw and Warneke, 2007) to form water clusters ($H_3O^+(H_2O)_n$) which levels depend on the relative humidity. A linear relationship was found between RH and the m/z 37-to-m/z 19 ratio (referred as m37/m19 ratio in the following) during laboratory tests (not shown).

2.3.2 NO_x artefact

OH radicals are artificially generated in the sampling reactor using a pen-ray Hg UV lamp from the photolysis of water. A drawback of this method is that a similar quantity of HO_2 is also generated since a hydrogen atom is formed in the water photolysis process, which then quickly reacts with O_2 to form HO_2. When ambient NO is sampled inside the reactor, these HO_2 radicals can be rapidly converted into OH radicals. This secondary formation of OH leads to differences in levels of OH between C2 and C3, and therefore to an artefact in the C3 measurement. To assess the correction to apply on C3 values, different amounts of NO (from 6 to 120 ppb) have been introduced inside the reactor while sampling humid zero air. These experiments have been conducted at different apparent pyrrole-to-OH ratios (from 1.6 to 3.9), determined by Eq. (2) and used to gauge the kinetic regime of the system. In practice, the pyrrole-to-OH ratio is adjusted by changing RH in the reactor.

$$\frac{\text{Pyrrole}}{\text{OH}} = \frac{\text{C1}}{\text{C1} - \text{C2}} \tag{2}$$

While NO_2 cannot lead to the formation of OH inside the reactor, its conversion into NO through photolysis or other chemical processes can also cause an artefact. To test the effect of NO_2 on C3 measurements, we followed the same procedure than described above for NO. Different amounts of NO_2 (from 60 to 410 ppb) have been introduced

AMTD
8, 3803–3850, 2015

inside the CRM reactor when sampling humid zero air at different pyrrole-to-OH ratios (from 1.6 to 3.2).

2.3.3 Deviation from pseudo first order kinetics

The measured OH reactivity values are calculated using Eq. (1). In this equation, pseudo first order conditions are assumed for pyrrole, i.e. pyrrole concentrations are at least several times higher than OH concentrations. However, operating conditions used on CRM instruments do not comply with this assumption and it is necessary to correct the calculated values (Eq. 1) for a deviation from pseudo first-order kinetics. To assess the artefact caused by this deviation, several gas standards (ethane, ethene, propane, propene, and isoprene) of known concentrations have been introduced inside the CRM reactor. It allows comparing the calculated OH reactivity generated by the standards (reactivity ranging from 6.5 to 65 s^{-1}) to the measured reactivity using Eq. (1). These experiments have been conducted at different pyrrole-to-OH ratios (from 1.4 to 2.6).

During these experiments, the C1 levels were of approximately 57 ppb (corresponding to a photolysis of 5 % of the 60.4 ppb of pyrrole introduced inside the reactor) and the C2 levels ranged from 17 to 43 ppb (corresponding to pyrrole-to-OH ratios ranging from 1.4 to 3.9).

3 Model descriptions

The laboratory tests performed in this study have been compared to results from zero-dimensional (0-D) box model simulations to test our understanding of the chemical processes occurring inside the reactor. These simulations have been conducted using two different mechanisms: a simple mechanism and the Master Chemical Mechanism v3.2 (http://mcm.leeds.ac.uk/MCM) (Jenkin et al., 1997, 2003, 2012; Saunders et al., 2003; Bloss et al., 2005). The two chemical mechanisms are presented in the following

AMTD
8, 3803–3850, 2015

section. The FACSIMILE solver was used to solve the differential equations generated from the different mechanisms. These simulations have been conducted constraining the box model by initial concentrations of Pyrrole, OH, and different standards used during the laboratory experiments. Both models were used to simulate the pyrrole modulations (C1-C2-C3).

Simulations are performed considering an ideal case where a finite amount of OH is introduced in a fresh mixture of air/standard trace gases, assuming a plug-flow in the reactor. In this scenario, (i) a small amount of OH is introduced in the air mixture, (ii) OH fully reacts with trace gases leading to oxidation products, (iii) the air mixture is refreshed at the OH injector tip before more OH is added. However, OH is produced continuously at the injector tip and OH can potentially react with byproducts and peroxy radicals previously formed since constant flows are maintained. While the simulation procedure used in this study may need some refinements, it is however interesting to compare trends observed during experimental tests to model simulations when some parameters such as the pyrrole-to-OH ratio are varied.

3.1 Simple mechanism

The simple mechanism (Table S2 in the Supplement) is an improved version of the mechanism used by Sinha et al. (2008) since it includes additional inorganic chemistry reactions from IUPAC 2001. The addition of these inorganic reactions aims at taking into account radical cross- and self-reactions (mainly $OH + HO_2$ and $HO_2 + HO_2$) as well as termination ($OH + NO_2$, $OH + NO$), and propagation reactions of NO_x with radicals, especially the reaction of HO_2 with NO which causes interferences in the OH reactivity measurements by generating secondary OH radicals.

Apart from these inorganic reactions, reactions of OH with pyrrole (1.2×10^{-10} cm^3 molecules^{-1} s^{-1}) and with a surrogate hydrocarbon (5.0×10^{-12} cm^3 molecules^{-1} s^{-1}) are included in the mechanism, both leading to a similar surrogate of organic peroxy radicals. In addition, reactions describing the chemistry of this surrogate RO_2 are included: $RO_2 + RO_2$, $RO_2 + HO_2$,

AMTD
8, 3803–3850, 2015

$RO_2 + NO = RO + NO_2$ and $RO + O_2 = HO_2$; reaction rate constants for these reactions are those for methylperoxy radical (CH_3O_2) ($3.4 \times \times 10^{-13}$, 5.2×10^{-12}; 7.7×10^{-12} and 1.9×10^{-15} cm^3 $molecules^{-1}$ s^{-1}, respectively). Inorganic and organic parts of this mechanism lead to a total number of reactions of 42.

3.2 The Master Chemical Mechanism (MCM)

A more comprehensive analysis of the chemistry occurring inside the CRM reactor has been conducted using the MCM v3.2. The use of a detailed mechanism such as the MCM aims at better representing the chemistry of peroxy radicals. Indeed, a detailed speciation of peroxy radicals that are formed during the oxidation of primary organic compounds is included in this mechanism. For this study, a MCM subset has been extract for inorganic reactions, ethane, propane, ethene, propene and isoprene. The 2(5H)-Furanone chemistry was also extracted to use it as a surrogate for the pyrrole chemistry since the latter is not included in the MCM. This subset of the MCM led to a mechanism containing 502 species and 1610 reactions.

The surrogate used for pyrrole, 2(5H)-Furanone ($C_4H_4O_2$), is named BZFUONE in the MCM. The choice of this surrogate has been made to be as close as possible of the pyrrole structure. It is also a cyclic compound but with an oxygen atom inside the ring instead of a nitrogen one. However, BZFUONE contains a carbonyl group in α position of the oxygen atom, which is not the case for pyrrole. We acknowledge that this is a crude approach to account for the pyrrole chemistry in the mechanism. There is no information about the pyrrole chemistry in the literature and a more rigorous approach was not possible. There is, therefore, a need of laboratory studies to investigate the photodegradation of pyrrole in atmospheric chambers.

The MCM was modified as the following. The reaction of pyrrole with OH leads to the formation of the same RO_2 than the reaction of BZFUONE with OH. However, the reaction rate constant has been set at the same value than in the simple mechanism (i.e. 1.2×10^{-10} cm^3 $molecules^{-1}$ s^{-1}). The same approach was done for the reaction

AMTD
8, 3803–3850, 2015

of pyrrole with O_3, using a rate constant of 1.57×10^{-17} cm^3 molecules^{-1} s^{-1} (Atkinson et al., 1984).

All the simulations have been conducted using operating conditions used during laboratory investigations: i.e. T = 20 °C, P = 760 Torr, except for the relative humidity (RH). Indeed, simulations have been performed for completely dry conditions (RH = 0 %) and for saturated conditions (RH = 100 %).

4 The Dunkirk field campaign

Preliminary OH reactivity measurements performed during a campaign which took place in an environment influenced by industrial, urban and marine air masses (Moderate to high NO_x) in Dunkirk (France) during July 2014 will be presented in Sects. 5.4 as an example to discuss raw data processing and uncertainties.

This campaign took place at a ground site located inside the harbour area of Dunkirk (51.0523° N; 2.3540° E) from 26 June to 31 July 2014. During this campaign, sequential measurements of OH reactivity and VOCs were performed with the MD-CRM instrument, especially designed for an identification of potential reactive species that are responsible for missing OH reactivity. Collocated measurements of 40 VOCs, inorganic species (NO_x, O_3, SO_2, CO, CO_2), meteorological parameters and aerosols were also performed. The results from this campaign will be presented in a forthcoming publication.

5 Results and discussions

In this section, experimental determinations of the different corrections applied to the MD-CRM measurements are presented, as well as the comparison to simulations conducted with the 0-D box models described above (see Sect. 3). Finally, we present

AMTD
8, 3803–3850, 2015

a detailed assessment of the limit of detection and the measurement uncertainties, as well as an example of data processing for a field campaign.

5.1 Correction for a change in RH between C2 and C3

Figure 2 shows the results of three experiments conducted to determine the sensitivity of C2 to humidity during the Dunkirk field campaign (summer 2014). The decrease of C2 with relative humidity is linear and can therefore be easily corrected during ambient measurements. A corrected C2 is recalculated for the RH value observed during the C3 measurement, taking into account its dependence to humidity (see Fig. 2) and the difference in the m37/m19 ratio monitored between C2 and C3 (see Eq. 3). In this equation, p corresponds to the slope of the linear regression between C2 and the m37/m19 ratio. The uncertainty on the determination of this slope has been estimated, from laboratory and field experiments, to be 12 %. The corrected C2 value is then used in Eq. (1) to calculate the OH reactivity.

$$C2_{corrected} = C2 + p\left[\left(\frac{m37}{m19}\right)_{C3} - \left(\frac{m37}{m19}\right)_{C2}\right] \quad (3)$$

The three experiments presented in Fig. 2 highlight the reproducibility of this determination over a period of ambient measurements longer than a month. In Fig. 2, the Black and red segments represent the mean and the maximum variation of m37/m19 between C2 and C3 during a field campaign in summer 2014, respectively. These segments illustrate the amplitude of the correction to apply on C2 values during ambient measurements.

AMTD
8, 3803–3850, 2015

5.2 NO_x interferences

5.2.1 Characterization of the NO interference – dependence on the Pyrrole-to-OH ratio

Figure 3 shows the results from experiments conducted to quantify the C3 dependence on NO due to OH formation from HO_2 + NO at different Pyrrole-to-OH ratios. The MD-CRM instrument was sampling humid zero air during these experiments. A total of 4 laboratory experiments (3 shown on Fig. 3) have been conducted at various Pyrrole-to-OH ratios (from 1.6 to 3.9) covering the typical range of ratios observed during ambient measurements (generally from 1.6 to 2.2).

The variation of C3 (ΔC3) is computed as the difference between an expected C3 and the measured C3, since a decrease in the pyrrole mixing ratio is expected with increasing NO mixing ratios. The expected C3 is calculated using measured levels of C1, C2 and expected OH reactivity due to NO (from 1.1 to 30.9 s^{-1}). Knowing these three terms, one can calculate the expected C3 from Eq. (1). To get an idea of the level of correction brought to the OH reactivity measurements, the absolute change in total OH reactivity for the experiment conducted at a pyrrole-to-OH ratio of 2.2 is also given in Fig. 3 (right axis).

As expected, a decrease of the pyrrole mixing ratio is observed when NO is introduced inside the reactor at a constant pyrrole-to-OH ratio. However, the variation of C3 with NO is not linear and varies with the Pyrrole-to-OH ratio. Indeed, the difference between the expected and measured C3 indicates a plateau at high NO mixing ratios. A quadratic regression forced through the origin is applied to fit the observations (solid lines in Fig. 3). Furthermore, the amplitude of the NO interference increases with the Pyrrole-to-OH ratio, i.e. with decreasing OH concentrations in the reactor, C1 being kept constant for all experiments.

It is interesting to note that the parameters from the quadratic regression evolved linearly with the Pyrrole-to-OH ratios (see bottom panels in Fig. 3). It is thus possible to interpolate the parameters from the quadratic regression to the Pyrrole-to-OH ratios

AMTD
8, 3803–3850, 2015

observed during field measurements to calculate the correction to apply to C3 due to NO interferences (see Eqs. 4–7):

$$C3^{corrected} = C3^{measured} + \Delta C3, \quad (4)$$

$$\text{With: } \Delta C3 = a[NO]^2 + b[NO], \quad (5)$$

$$\text{With: } a = a_1 \frac{\text{Pyrrole}}{\text{OH}} + a_2 \text{ and } b = b_1 \frac{\text{Pyrrole}}{\text{OH}} + b_2, \quad (6)$$

$$\text{So: } \Delta C3 = \left(a_1 \frac{\text{Pyrrole}}{\text{OH}} + a_2\right)[NO]^2 + \left(b_1 \frac{\text{Pyrrole}}{\text{OH}} + b_2\right)[NO]. \quad (7)$$

Results of the experiment performed using dry zero air (Pyrrole-to-OH ratio of 3.9) is not taken into account in the linear fits presented in the bottom panels of Fig. 3 because a deviation from the linearity is observed. Not considering this point is acceptable since completely dry conditions are never observed in ambient measurements, and observed Pyrrole-to-OH ratios are always lower than 2.6 in ambient air. These experiments have also been carried out by adding different standards in the reactor at the same time than NO (for OH reactivity values, due to the standard additions, ranging from 22.2 to 36.6 s^{-1}). These experiments and the discussion on the effect of adding a VOC (ethane, isoprene) are shown in the Supplement (Fig. S2). Briefly, no clear impact has been found on the NO interferences, suggesting that the correction characterized above is suitable for ambient measurements. The correction can be applied during field measurements using the pyrrole-to-OH ratio continuously monitored by the CRM instrument and the measured ambient NO mixing ratios.

5.2.2 Impact of NO_2

Figure 4 (Top panel) displays the changes in C3 with NO_2 mixing ratios inside the reactor for three different Pyrrole-to-OH ratios. As for NO, the introduction of NO_2 in the reactor leads to a decrease of the pyrrole mixing ratio. The changes in C3 appear to be also non-linear showing a plateau at high NO_2 mixing ratios (above approximately

AMTD
8, 3803–3850, 2015

150 ppb of NO_2 in the reactor). However, no clear difference is observed for experiments conducted at various Pyrrole-to-OH ratios.

The interference caused by NO_2 may be due to its conversion into NO before or within the reactor. To determine the fraction of NO_2 converted into NO, we calculated the amount of NO needed (based on the experiments presented in Sect. 5.2.1) to explain the changes observed on C3 when NO_2 was introduced inside the reactor. From all the experiments conducted with this set up, these calculations led to a conversion ranging from 15.5 to 37 %, with an average value of 24 % (±9 %, 1σ), see Fig. 4 bottom panel.

Further work was performed to study the conversion of NO_2 inside MD-CRM, a NO_x analyzer (Thermo Environmental Instruments, model 42C) has been connected to the reactor exhaust instead of the PTR-MS while NO_2 was introduced at the reactor inlet. Since the sampling flow rate of the NO_x analyzer was 600 sccm, 460 sccm of zero air was added in the sampling line of the NO_x analyzer to only sample 140 sccm from the reactor, similar to the sampling flow rate from the PTR-MS instrument. Large mixing ratios of NO were observed at the exit of the reactor (between 25 and 30 % of total NO_x) when the mercury lamp was OFF, while low NO mixing ratios (~ 8.7 % of total NO_x) was observed at the reactor inlet. This result indicates that NO_2 is not converted into NO by photolysis but rather by heterogeneous chemical processes, probably on stainless steel pieces upstream and downstream the glass reactor. The replacement of all the stainless steel pieces in the set-up is planned in the future to avoid, or at least to reduce, this NO_2 conversion.

Using a similar approach than for NO, the correction to apply on C3 for NO_2 can be calculated using a quadratic regression shown in Fig. 4, independently of the pyrrole-to-OH ratio, using the measurements of ambient NO_2. It is worthwhile noting that the amplitude of the correction is much lower for NO_2 than for NO.

AMTD
8, 3803–3850, 2015

5.2.3 Comparison of laboratory observations to model simulations

To understand the chemical processes occurring inside the CRM reactor, we compared 0-D box model simulations to the experimental observations discussed above. It is worth noting that the pyrrole-to-OH ratios reported for the simulations were calculated the same way than during the experiments, i.e. using Eq. (2). However, the calculations do not lead to the real pyrrole-to-OH ratios but to apparent ratios, characteristic of the amount of OH reacting with pyrrole. Since the mechanisms include self and cross reactions of radicals, all the OH introduced in the model does not react with pyrrole, and true pyrrole-to-OH ratios are lower than the measured apparent ratios. A comparison of real and apparent ratios is given in Fig. S3. For instance, an apparent pyrrole-to-OH ratio of 2 is characteristic of a real pyrrole-to-OH ratio of approximately 1 for simulations conducted under dry conditions with the simple mechanism and same initial quantities of OH and HO_2.

The initial mixing ratios of OH in the simulations have been set to reproduce the apparent pyrrole-to-OH ratios observed during the experiments. The real mixing ratios of OH inside the reactor have also been determined experimentally and compared to the levels set in the model and the fraction of OH reacting with Pyrrole (estimated from C1–C2) (Fig. S4). OH mixing ratios set in the model agree within uncertainties with the experimental determinations, showing that initial conditions used in the model are representative of the real OH mixing ratios inside the reactor.

Experimental results related to the NO interference, as well as simulations performed using both mechanisms described in Sect. 3 (the simple mechanism and the MCM), are displayed in Fig. 5.

The models predict a similar change in C3 than the experiments when NO increases inside the reactor. Indeed, the models predict that ΔC3 first increases with NO and levels off after the addition of a certain amount (> 90 ppbv). This behavior indicates that when a critical concentration of NO is reached, all HO_2 radicals are titrated and a further increase of NO does not cause any additional formation of OH through the

AMTD
8, 3803–3850, 2015

$NO + HO_2$ reaction. Furthermore, the models also predict that ΔC3 becomes larger at higher pyrrole-to-OH ratios, similar to the experimental observations. A potential reason for this behavior is that the concentrations of both OH and HO_2 are lower at higher pyrrole-to-OH ratios, since the pyrrole concentration is held constant in all experiments and simulations (C1 = 55 ppb). Lower concentrations of radicals lead to a slower reaction rate between OH and HO_2. So, the OH formed from reaction between HO_2 and NO, even in lower quantity, will preferentially react with pyrrole rather than HO_2, leading to a larger change in ΔC3.

Significant differences are found between the simulations conducted using the two mechanisms. Indeed, simulations performed using the simple mechanism leads to an overestimation of the NO interference by up to 27 % while simulations performed using the MCM leads to an underestimation by up to 10 %. The differences between both mechanisms lie in the way the chemistry of organic peroxy radicals is treated. In the simple mechanism, each reaction of OH with an organic compound gives the same RO_2 radical, which propagates to HO_2 after reaction with NO and O_2 with no stable compound formed as byproduct. In the MCM, a more complex chemistry is included since specific peroxy radicals are formed for each reacting organic molecule and stable byproducts are generated from the peroxy radical reactions, which can further react with OH. Since, the simulations from both mechanisms encompass the experimental results, one can conclude than the lack of speciation for RO_2 radicals and of secondary chemistry in the simple mechanism do not allow to reproduce the observations, while the secondary chemistry included in the MCM, in particular the proxy used to account for the pyrrole chemistry (BZFUONE), is not fully representative of the chemistry involved in the CRM reactor. Therefore, a detailed study of the chemistry of the oxidation of pyrrole is needed to fully understand the processes occurring in the CRM reactor.

It is interesting to note that both mechanisms lead to coefficients (a and b) of the quadratic regressions (ΔC3 vs. pyrrole-to-OH) similar to that observed for the laboratory experiments (see bottom panels of Fig. 5).

AMTD
8, 3803–3850, 2015

Since all the simulations described above have been conducted under dry conditions, the influence of humidity on simulation results has been tested by reproducing the same simulations with a relative humidity of 100 % (Fig. S5). A decrease of ΔC3 of less than 10 % is observed at all pyrrole-to-OH ratios. This can be explained by an enhancement of the rate of the HO_2 self-reaction in the presence of water, reducing the secondary formation of OH, hence the NO interference. In practice, the pyrrole-to-OH ratios are directly linked to the relative humidity inside the reactor, since OH levels depend on the amount of water available for photolysis. Thus, the correct simulation results to compare to the experimental results are between these two extreme cases (dry and RH saturated), being closer to dry condition results at higher Pyrrole-to-OH ratios and vice versa. However, only small differences are observed and the conclusions made by simulating dry conditions are valid.

The effect of standard additions (Isoprene and Ethane) in the simulations has also been tested and is displayed in Fig. S6. The simulations using the MCM mechanism suggests a small dependence on ΔC3 ($\sim 6.1 \pm 1.1$ %) for an OH reactivity due to VOCs of 20–40 s^{-1}, especially at high NO concentrations (NO > 100 ppb). This difference is small and will be within the measurement uncertainties.

The simulations presented above have been performed assuming no O_3 in the reactor. However, photolysis of O_2 may occur inside the reactor using Hg pen ray UV lamp leading to a significant O_3 concentration. The influence of O_3 on simulated NO artefacts has been tested, initializing O_3 concentration to 200 ppb in the simulations using the MCM mechanism (Fig. S12.2). The 200 ppb of ozone correspond to the measured value at the exhaust of the reactor under dry conditions, using an ozone analyzer (Environnement-SA, model O3-42M). Briefly, the impact of adding 200 ppb of ozone in the simulations leads to a small decrease of the NO artefact by approximately 2.5 %, independent of the pyrrole-to-OH ratio. It is interesting to note that the presence of hundreds of ppb of ozone in the reactor might also leads to a production of OH trough ozone photolysis, producing O^1D, which quickly reacts with H_2O to form two OH radi-

AMTD
8, 3803–3850, 2015

cals. Therefore, the OH present in the reactor might come not only from H_2O photolysis but also from O_3 photolysis.

5.3 Correction for a deviation from pseudo first order kinetics

The corrected values of C2 (Eq. 3) and C3 (Eq. 4) are used in Eq. (1) to calculate the OH reactivity. As mentioned previously, Eq. (1) was derived based on the assumption that the reactions occur under first-order kinetic conditions with respects to pyrrole and ambient trace gases. However, as discussed above, this assumption is not fulfilled since the OH mixing ratio inside the reactor is on the same magnitude than the pyrrole mixing ratio. The correction applied on the calculated OH reactivity to account for this deviation is described below.

5.3.1 Experimental characterization of the correction to apply to account for a deviation from pseudo first order kinetics – dependence on the pyrrole-to-OH ratio

Figure 6 displays experimental observations of the measurement bias caused by a deviation from pseudo first-order kinetics. This figure compares the OH reactivity values calculated from the addition of a gas standard to the values measured by the MD-CRM instrument, using Eq. (1), and corrected for changes in humidity between C2 and C3 (see Sect. 5.1). NOx species were not added in these experiments.

The top panel of Fig. 6 shows results from the addition of three different standards (isoprene, ethane, and propene), characterized by OH rate constants spanning almost 3 orders of magnitude (1.0×10^{-10}, 2.4×10^{-13}, 2.9×10^{-11} $cm^3\,molecules^{-1}\,s^{-1}$ respectively), at a pyrrole-to-OH ratio of 1.4. This figure indicates a linear relationship between the measured and the calculated OH reactivity. The slope F of a linear regression represents the correction factor to apply to the measured OH reactivity values (see Eq. 8):

$$R_{OH}^{true} = F \times R_{OH}^{measured}, \quad (8)$$

AMTD
8, 3803–3850, 2015

where R_{OH}^{true} represents the calculated total OH reactivity, knowing the concentration and the reaction rate constants with OH of the gas standards added in the reactor, and $R_{OH}^{measured}$ represents the OH reactivity measured by the MD-CRM instrument and corrected for changes in relative humidity between C2 and C3. For ambient measurements, R_{OH}^{true} will represent the measured OH reactivity corrected for a deviation from pseudo first order kinetics.

The correction factors determined at a pyrrole-to-OH ratio of 1.4 indicate that the reactivity of the standard plays a role in the observed bias. Higher correction factors are found for more reactive compounds. Indeed, at a pyrrole-to-OH ratio of 1.4, the correction factor determined for isoprene is 7.6 % higher than for propene and is 50.6 % higher than for ethane. However, the middle panel of Fig. 6 indicates that the differences observed between the different gas standard are lower at a pyrrole-to-OH ratio of 2.3, with the correction factor derived for isoprene being only 1 % different than for ethane, which is not significant.

Experiments performed at various pyrrole-to-OH ratios (4 ratios: 1.4, 1.6, 1.8, 2.3, not shown) indicate that the relative differences between correction factors determined using ethane and isoprene range from 1–57.8 % and confirms the strong dependence on the pyrrole-to-OH ratio, with negligible differences for ratios higher than 2.3. These two standards represent extreme cases since ethane is one of the less reactive VOC in the atmosphere (reaction rate constant with OH: 2.4×10^{-13} cm^3 molecules^{-1} s^{-1}) while isoprene is one of the most reactive (reaction rate constant with OH: 1.0×10^{-10} cm^3 molecules^{-1} s^{-1}). It is interesting to note that ambient air is a mixture of a large number of compounds with reaction rate constants ranging between that of ethane and isoprene. The correction factor should therefore be calculated as an averaged correction factor determined using different standards covering the full range of reaction rate constants.

Results from the addition of the same standard (isoprene) at three different pyrrole-to-OH ratios (1.4, 1.8, and 2.3) are shown in the bottom panel of Fig. 6. The correction factors derived from these experiments increases when the pyrrole-to-OH ratio

AMTD
8, 3803–3850, 2015

decreases. Indeed, the highest correction factor (1.59) is found for the lowest pyrrole-to-OH ratio (i.e. 1.4 here) and the lowest correction factor (0.84) is found for the highest Pyrrole-to-OH ratio (i.e. 2.3 here). Since, the pyrrole concentration is kept constant, an increase of the Pyrrole-to-OH ratio is a result of a decrease of the OH concentration (due to a decrease of RH). A decrease of the correction factor with the pyrrole-to-OH ratio is consistent with a kinetic regime getting closer to pseudo first-order conditions (OH $\gg$ Pyrrole). However, we observed that the correction factors determined experimentally seems to decrease to values lower than unity at pyrrole-to-OH ratios higher than 2.3. However, this tendency is only significant for one experiment performed at a pyrrole-to-OH ratio of 2.6. One could expect that while the pyrrole-to-OH ratio increases, the kinetic regime gets closer to pseudo first-order conditions, and thus the correction factor should tend to unity. This discrepancy is further discussed in the model-experiment comparison section.

Results from the addition of other gas standards (ethene, $k = 8.5 \times \times 10^{-12}$ cm^3 molecules^{-1} s^{-1} and propane, $k = 1.09 \times \times 10^{-12}$ cm^3 molecules^{-1} s^{-1}) in the reactor are consistent with the results shown in Fig. 6 and confirmed the different trends discussed above (Fig. S7).

From these experiments, it appears essential to take into account the pyrrole-to-OH ratio in the correction to apply to the measured reactivity values. Figure 7 shows how the correction factor varies with the pyrrole-to-OH ratio. The correction factors shown in this figure were derived from single experiments using different standards (ethane, ethene, propane, propene, and isoprene) (as shown in Fig. 6). This figure gather laboratory and field experiments performed over 7 months. The gas standards were chosen to cover a large range of reaction rate constants with OH (from 2.4×10^{-13} cm^3 molecules^{-1} s^{-1} for ethane to 1.0×10^{-10} cm^3 molecules^{-1} s^{-1} for isoprene) to take into account the impact of the gas reactivity on the correction factor.

From the linear relationship observed in Fig. 7, the correction factor to apply to the measurements can be calculated from the pyrrole-to-OH ratio that is monitored during

AMTD
8, 3803–3850, 2015

field or laboratory measurements using Eq. (9):

$$F = -0.16\mathrm{Pyr/OH} + 1.27. \quad (9)$$

Within the small range of pyrrole-to-OH ratios generally encountered during field campaigns, typically from 1.6 to 2.2, the correction factors, determined using Eq. (9), range between 0.9 and 1.0. Therefore, an averaged value of the correction factors can be considered instead of using a pyrrole-to-OH dependent correction factor (see Fig. 7). It is interesting to note that this correction takes into account the deviation from pseudo first order kinetics but also any unknown artefact impacting the measurements of OH reactivity inside the reactor, such as radical segregation and wall losses of radicals.

5.3.2 Comparison of laboratory observations to model simulations

Simulations performed using both mechanisms presented in Sect. 3 (the simple mechanism and the MCM) as well as a mechanism similar to the one described by Sinha et al. (2008), which does not take into account radical-radical reactions, are displayed in Fig. 8.

The top panel of Fig. 8 displays the results from the addition of three different standards (isoprene, ethane, propene) using the MCM mechanism and a surrogate standard for the simple mechanism, characterized by different reaction rate constants with OH (1.0×10^{-10}, 2.4×10^{-13}, 2.9×10^{-11}, and 5.0×10^{-12} $\mathrm{cm^3\,molecules^{-1}\,s^{-1}}$, respectively), at a pyrrole-to-OH ratio of 1.4. It is interesting to note that simulations performed using MCM for a gas standard exhibiting an OH rate constant of 5.0×10^{-12} $\mathrm{cm^3\,molecules^{-1}\,s^{-1}}$ are similar to that observed with the simple mechanism, suggesting that the detailed secondary chemistry included in MCM is not important to model this correction. These results show that the correction factor should increase with the OH rate constant, independently of the mechanism used (the MCM or the simple mechanism). This trend is consistent with the observations made during laboratory experiments (see Sect. 5.3.1).

AMTD
8, 3803–3850, 2015

Simulations conducted with the simple mechanism and the mechanism from Sinha et al. (2008) (called 2-reaction mechanism) are presented in the bottom panel of Fig. 8 for a surrogate gas standard ($k = 5.0 \times 10^{-12}$ cm^3 molecules^{-1} s^{-1}) at three different pyrrole-to-OH ratios (1.4, 1.9, and 2.9). The correction factor derived from the simulations performed using the simple mechanism decreases with increasing pyrrole-to-OH ratios as observed during the laboratory experiments. As mentioned previously, these observations are consistent with a chemical system getting closer to pseudo first order kinetic conditions (OH $\ll$ Pyrrole) when the pyrrole-to-OH ratio increases. In contrast, an opposite trend is observed when the mechanism "2-reaction mechanism" is used. This result highlights the importance of taking into account radical-radical reactions in the mechanism to describe the complex chemistry occurring in the reactor.

Both mechanisms, the simple mechanism and MCM, lead to correction factors that are converging to unity when pyrrole-to-OH increases (i.e. OH decreases). This result differs from experimental observations, since experimental correction factors are lower than unity at high pyrrole-to-OH ratios.

Figure 9 (Top panel) shows how the correction factor changes with the pyrrole-to-OH ratio. The simulated values stem from the simulations conducted using the box model including the MCM mechanism and constrained with ethane or isoprene under dry conditions, as well as under wet conditions (RH = 100 %) for ethane. The simulated correction factors for ethane under dry conditions are higher than the measurements by 72 and 54 % at pyrrole-to-OH ratios of 1.4 and 1.9, respectively. These differences are even larger (143 and 80 % at pyrrole-to-OH ratios of 1.4 and 1.9, respectively) for isoprene. However, a similar behavior is observed: i.e. a decrease of the correction factors with increasing pyrrole-to-OH ratios. Performing simulations in presence of water improve the agreement but still fails short to reconcile simulations and measurements. Furthermore, 100 % of relative humidity is not likely inside the reactor, and the real conditions are between these two extreme cases.

Several hypotheses (segregation in the reactor, RO_2 + OH reactions (Fittschen et al., 2014), uncertainties in reaction rate constants of radical-radical reactions, higher or

AMTD
8, 3803–3850, 2015

lower proportions of HO_2 compared to OH inside the reactor, presence of O_3 inside the reactor) have been tested in the simulations to try to reconcile simulated results and laboratory observations (see Sects. S8–S13). Unfortunately, none of these hypotheses seems to explain totally the disagreement, even if the uncertainty in reaction rate constants of radical-radical reactions and the possible lower proportion of HO_2 inside the reactor allow improving the agreement between simulations and measurements. The combination of these two hypothesis (lower proportion of HO_2 by 25 % and reaction rate constants of reaction between OH and HO_2 reduced by 20 %) leads to even closer agreement (within 15 %) between measurements and simulations (not shown), but the issue concerning correction factors below unity at high pyrrole-to-OH ratios observed during laboratory experiments still cannot be reproduced by the model.

This inability of the model to reproduce the laboratory observations may be due to the approach used to perform the simulations (see Sect. 3), a potential lack of knowledge in the secondary chemistry from pyrrole oxidation products, and an impact of the flow dynamic inside the reactor. An investigation of the chemistry of pyrrole would help to better understand the processes occurring in the reactor. Furthermore, the coupling of the chemical mechanism with a CFD (Computational Fluid Dynamics) model would be helpful. It would help considering a constant production of OH from the injector and the reaction of OH with byproducts and peroxy radicals previously formed inside the reactor.

Nevertheless, the similar behaviors observed between simulations and experiments give confidence in the experimental determinations of the correction factors. It is worth noting that the dependence of the correction factor to the reactivity of added gas standards decreases at higher pyrrole-to-OH ratios (see Fig. 9, bottom panel). A similar trend is observed for the water dependence of the correction factor. It would therefore be beneficial to run the CRM instruments at high pyrrole-to-OH ratios to reduce the uncertainty introduced by the correction applied to account for a deviation from pseudo first-order kinetics, keeping in mind that a higher pyrrole-to-OH ratio leads to a lower

AMTD
8, 3803–3850, 2015

OH mixing ratio in the reactor and thus a higher detection limit. Working at pyrrole-to-OH ratios ranging from 1.7–2.0 seems to be optimal for the MD-CRM instrument.

5.4 Limit of detection and measurement uncertainties

The Limit of detection (LOD) indicates the minimal detectable difference between C2 and C3. The LOD was determined keeping the CRM instrument under C2 conditions for 15 h during the Dunkirk field campaign, July 2014 (see Sect. 4). This 15 h segment was then split into subsets of 5 min to calculate a SD (σ_{C2}) for each subset and an averaged value of the SD throughout the whole time period ($\overline{\sigma_{C2}}$). This approach was used to avoid the variability in C2 measurements due to changes in ambient relative humidity, which drives the zero air humidity. An OH reactivity value was then calculated using the measured C1 value, an averaged C2 value ($\overline{C2}$), and 3 times the average SD calculated above (i.e. $C3 = \overline{C2} + 3\overline{\sigma_{C2}}$) at an averaged pyrrole-to-OH ratio of 1.7. The calculated OH reactivity value, characteristic of the LOD at 3σ, was 3.0 s^{-1} for the MD-CRM instrument.

To assess the total uncertainty of the OH reactivity measurements, we need to consider a propagation of uncertainties from all the parameters included in the OH reactivity calculation (Eq. 1), including the corrections. A detailed description of this approach is given in Sect. S14.

An example of precision values (random error) and total uncertainty values, taking into account different levels of corrections, is given as a function of total OH reactivity measurements in Fig. 10 (top panel) for the Dunkirk field campaign.

The precision (purple dots in the Top panel) is dependent on the OH reactivity level and ranges from approximately 50 % at the LOD of 3 s^{-1} to less than 4 % at OH reactivity values higher than 50 s^{-1}. When systematic errors, except those associated to the humidity and NO corrections, are accounted for in the total uncertainty calculation (blue dots), the total uncertainty levels off at approximately 17.5 % for OH reactivity values higher than 15 s^{-1}, while a low impact is observed at lower OH reactivity values.

AMTD
8, 3803–3850, 2015

This is consistent with the systematic errors and the measurement precision driving the uncertainty at high and low OH reactivity levels, respectively.

Including uncertainties due to the correction for humidity changes between C2 and C3 (green open dots) has a small impact on the total uncertainty and only small differences are observed (1.5 ± 3.0 % of relative differences on average). Finally, including uncertainties due to the correction for NO interferences (red open dots) leads to a sharp increase of the total uncertainty for data points characterized by elevated NO mixing ratios (7.3 ± 39.8 % of relative differences on average).

Figure 10 (bottom panel), shows the total uncertainty, including all sources of errors (precision, systematic errors, corrections), as a function of total OH reactivity and color-coded by NO_x levels. The largest uncertainties are found for high NO_x levels (from 20 to 120 ppb). The total uncertainty for OH reactivity values higher than 15 s^{-1} depends strongly on NO and is in ranges from 17.5–25 % at NO_x mixing ratios < 30 ppb; 25–70 % at NO_x mixing ratios of 30–80 ppb; and can be as high as 200 % at NO_x levels above 80 ppb, depending on the total OH reactivity level.

The time series of ambient OH reactivity measurements at different stage of the data processing are presented in Fig. 11 for the Dunkirk field campaign, showing the amplitudes of the different corrections.

In moderate to rich NO_x environments such as the Dunkirk site the correction for NO_x has the largest impact on OH reactivity measurements. The correction that has the second largest impact is the correction for Humidity. On average, a significant correction of 5.2 s^{-1} is observed due to fast changes in ambient RH (proximity of the sea), causing differences in humidity between C2 and C3 steps separated by 10 min intervals. Other corrections are less important even if they are non-zero. It is interesting to note that the accuracy of this approach to correct the OH reactivity measurements on the MD-CRM instrument has been tested in Hansen et al. (2015) and has been found to be suitable for NO_x mixing ratios up to 70–100 ppbv.

AMTD
8, 3803–3850, 2015

6 Conclusion

This study presents the results of an exhaustive characterization of a CRM instrument developed at Mines Douai to measure total OH reactivity in the troposphere. This characterization aimed at assessing the different corrections that need to be applied during data processing and to get more insights into the chemical processes occurring inside the CRM reactor. To do so, a suite of laboratory experiments has been conducted and the results have been compared to simulations from a 0-D box model including a simple chemical mechanism made of 42 reactions or a more exhaustive chemical mechanism based on a subset of the Master Chemical Mechanism (MCM) made of 1610 reactions.

As previously reported in the literature, artefacts in total OH reactivity measurements have been identified from changes in humidity between the C2 and C3 measurements, from the spurious formation of OH through the $HO_2 + NO$ reaction, and from a deviation from pseudo first order kinetics. The correction to apply for changes in humidity between C2 and C3 can easily be assessed by monitoring the dependence of C2 with a proxy for humidity, e.g. m37/m19 on PTR-MS instruments.

A quadratic parameterization has been developed to correct the OH reactivity measurements for the NO interference by characterizing the C3 sensitivity to NO and the Pyrrole-to-OH ratio during laboratory experiments. Changes in C3 levels have been found to increase and level off with NO concentrations and to increase with pyrrole-to-OH ratios. C3 has also been found to be sensitive to NO_2. This NO_2 dependence has been attributed to a conversion of NO_2 into NO of approximately 24 %, occurring mainly on surfaces and not due to photolysis in the reactor. This unwanted conversion will be carefully investigated to eliminate it or to reduce it at a negligible level.

The correction to apply for a deviation from pseudo first-order kinetics can be assessed by performing calibrations using different trace gases exhibiting different reaction rate constants with OH and at different pyrrole-to-OH ratios, since dependences of the correction factor on the bimolecular rate constant of the gas standard and on the pyrrole-to-OH ratio have been observed experimentally. We recommend using an

AMTD
8, 3803–3850, 2015

average correction factor derived from calibrations made using different standards and to develop a parameterization depending on the Pyrrole-to-OH ratio.

The simulations performed using both mechanisms reproduced the magnitude of the corrections for the NO interference and the deviation from pseudo first order kinetics, as well as the dependences on Pyrrole-to-OH ratios and bimolecular rate constants of the gas standards. The reasonable agreement observed between simulations and experiments give confidence in the parameterizations proposed in this study. However, it would be hazardous to use the numeric values of the parameterizations proposed in this study for other CRM instruments and it is recommended that each group characterizes its own instrument. It is interesting to note that a comparison of the corrections needed on different CRM instruments would help investigating the robustness of this technique.

However, remaining differences between simulations and experimental results point out the need of a better understanding of the pyrrole chemistry. Studies are needed to investigate the oxidation chemistry of this compound. In addition, it would be worth coupling a CFD model to the chemical mechanisms described in this work to investigate the impact of flow dynamics on the CRM measurements, which in turn would provide a better description of the complex processes occurring in the reactor.

Finally, the CRM instrument developed at Mines Douai has already been successfully deployed in the field giving satisfactory results in variable environments. A good agreement during intercomparison exercises with other instruments: another CRM instrument and a Pump-Probe instrument have been found, highlighting the suitability of the proposed corrections for the CRM technique.

The Supplement related to this article is available online at doi:10.5194/amtd-8-3803-2015-supplement.

Acknowledgements. The authors are grateful to J. Williams (MPIC-Mainz) for providing a spare CRM glass reactor, V. Sinha (IISER-Mohali) for his assistance during the development of

AMTD
8, 3803–3850, 2015

the MD-CRM instrument, and Stephane Sauvage for helpful discussions about the assessment of measurement uncertainties. This research was funded by the European Union Seventh Framework Programme under Grant Agreement number 293897, "DEFIVOC" project and by the CaPPA project. The CaPPA project (Chemical and Physical Properties of the Atmosphere) is funded by the French National Research Agency (ANR) through the PIA (Programme d'Investissement d'Avenir) under contract "ANR-11-LABX-0005-01" and by the Regional Council Nord-Pas de Calais and the "European Funds for Regional Economic Development" (FEDER). R. F. Hansen's internship in Mines Douai was supported by a Chateaubriand Science Fellowship from the French Embassy of the United States. The authors also want to thank all colleagues involved in the field deployments of the MD-CRM instrument.

References

Atkinson, R., Aschmann, S. M., Winer, A. M., and Carter, W. P. L.: Rate constants for the gas phase reactions of OH radicals and O_3 with pyrrole at 295 ± 1 K and atmospheric pressure, Atmos. Environ., 18, 2105–2107, doi:10.1016/0004-6981(84)90196-3, 1984.

Bloss, C., Wagner, V., Jenkin, M. E., Volkamer, R., Bloss, W. J., Lee, J. D., Heard, D. E., Wirtz, K., Martin-Reviejo, M., Rea, G., Wenger, J. C., and Pilling, M. J.: Development of a detailed chemical mechanism (MCMv3.1) for the atmospheric oxidation of aromatic hydrocarbons, Atmos. Chem. Phys., 5, 641–664, doi:10.5194/acp-5-641-2005, 2005.

Calpini, B., Jeanneret, F., Bourqui, M., Clappier, A., Vajtai, R., and van den Bergh, H.: Direct measurement of the total reaction rate of OH in the atmosphere, Analusis, 27, 328–336, doi:10.1051/analusis:1999270328, 1999.

Carslaw, N., Creasey, D. J., Heard, D. E., Jacobs, P. J., Lee, J. D., Lewis, A. C., McQuaid, J. B., Pilling, M. J., Bauguitte, S., Penkett, S. A., Monks, P. S., and Salisbury, G.: Eastern Atlantic Spring Experiment 1997 (EASE97) – 2. Comparisons of model concentrations of OH, HO_2, and RO_2 with measurements, J. Geophys. Res., 107, 4190, doi:10.1029/2001JD001568, 2002.

De Gouw, J. and Warneke, C.: Measurements of volatile organic compounds in the Earth's atmosphere using proton-transfer reaction mass spectrometry, Mass Spectrom. Rev., 26, 223–257, 2007.

AMTD
8, 3803–3850, 2015

Di Carlo, P., Brune, W. H., Martinez, M., Harder, H., Lesher, R., Ren, X., Thornberry, T., Carroll, M. A., Young, V., Shepson, P. B., Riemer, D., Apel, E., and Campbell, C.: Missing OH reactivity in a forest: evidence for unknown reactive biogenic VOCs, Science, 304, 722–725, doi:10.1126/science.1094392, 2004.

Dillon, T., Tucceri, M., Dulitz, K., Horowitz, A., Vereecken, L., and Crowley, J.: Reaction of hydroxyl radicals with C_4H_5N (Pyrrole): temperature and pressure dependent rate coefficients, J. Phys. Chem. A, 116, 6051–6058, doi:10.1021/jp211241x, 2012.

Dolgorouky, C., Gros, V., Sarda-Esteve, R., Sinha, V., Williams, J., Marchand, N., Sauvage, S., Poulain, L., Sciare, J., and Bonsang, B.: Total OH reactivity measurements in Paris during the 2010 MEGAPOLI winter campaign, Atmos. Chem. Phys., 12, 9593–9612, doi:10.5194/acp-12-9593-2012, 2012.

Dusanter, S., Vimal, D., Stevens, P. S., Volkamer, R., Molina, L. T., Baker, A., Meinardi, S., Blake, D., Sheehy, P., Merten, A., Zhang, R., Zheng, J., Fortner, E. C., Junkermann, W., Dubey, M., Rahn, T., Eichinger, B., Lewandowski, P., Prueger, J., and Holder, H.: Measurements of OH and HO_2 concentrations during the MCMA-2006 field campaign – Part 2: Model comparison and radical budget, Atmos. Chem. Phys., 9, 6655–6675, doi:10.5194/acp-9-6655-2009, 2009.

Fittschen, C., Whalley, L. K., and Heard, D. E.: The reaction of CH_3O_2 radicals with OH radicals: a neglected sink for CH_3O_2 in the remote atmosphere, Environ. Sci. Technol., 48, 14, 7700–7701, 2014.

Goldstein, A. H. and Galbally, I. E.: Known and unexplored organic constituents in the earth's atmosphere, Environ. Sci. Technol., 41, 1514–1521, 2007.

Hansen, R. F., Griffith, S. M., Dusanter, S., Rickly, P. S., Stevens, P. S., Bertman, S. B., Carroll, M. A., Erickson, M. H., Flynn, J. H., Grossberg, N., Jobson, B. T., Lefer, B. L., and Wallace, H. W.: Measurements of total hydroxyl radical reactivity during CABINEX 2009 – Part 1: field measurements, Atmos. Chem. Phys., 14, 2923–2937, doi:10.5194/acp-14-2923-2014, 2014.

Hansen, R. F., Blocquet, M., Schoemaecker, C., Léonardis, T., Locoge, N., Fittschen, C., Hanoune, B., Stevens, P. S., Sinha, V., Dusanter, S.: Intercomparison of the Comparative Reactivity Method (CRM) and pump-probe technique for measuring total OH reactivity in an urban environment, Atmos. Meas. Tech. Discuss., in preparation, 2015.

Hofzumahaus, A., Rohrer, F., Lu, K. D., Bohn, B., Brauers, T., Chang, C. C., Fuchs, H., Holland, F., Kita, K., Kondo, Y., Li, X., Lou, S. R., Shao, M., Zeng, L. M., Wahner, A., and

AMTD
8, 3803–3850, 2015

Zhang, Y. H.: Amplified trace gas removal in the troposphere, Science, 324, 1702–1704, 2009.
Jenkin, M. E., Saunders, S. M., and Pilling, M. J.: The tropospheric degradation of volatile organic compounds: a protocol for mechanism development, Atmos. Environ., 31, 81–104, 1997.
Jenkin, M. E., Saunders, S. M., Wagner, V., and Pilling, M. J.: Protocol for the development of the Master Chemical Mechanism, MCM v3 (Part B): tropospheric degradation of aromatic volatile organic compounds, Atmos. Chem. Phys., 3, 181–193, doi:10.5194/acp-3-181-2003, 2003.
Jenkin, M. E., Wyche, K. P., Evans, C. J., Carr, T., Monks, P. S., Alfarra, M. R., Barley, M. H., McFiggans, G. B., Young, J. C., and Rickard, A. R.: Development and chamber evaluation of the MCM v3.2 degradation scheme for β-caryophyllene, Atmos. Chem. Phys., 12, 5275–5308, doi:10.5194/acp-12-5275-2012, 2012.
Kim, S., Guenther, A., Karl, T., and Greenberg, J.: Contributions of primary and secondary biogenic VOC tototal OH reactivity during the CABINEX (Community Atmosphere-Biosphere INteractions Experiments)-09 field campaign, Atmos. Chem. Phys., 11, 8613–8623, doi:10.5194/acp-11-8613-2011, 2011.
Kovacs, T. A. and Brune, W. H.: Total OH loss rate measurement, J. Atmos. Chem., 39, 105–122, doi:10.1023/A:1010614113786, 2001.
Levy, H.: Photochemistry of the lower troposphere, Planet. Space Sci., 20, 919–935, 1972.
Lou, S., Holland, F., Rohrer, F., Lu, K., Bohn, B., Brauers, T., Chang, C.C., Fuchs, H., Häseler, R., Kita, K., Kondo, Y., Li, X., Shao, M., Zeng, L., Wahner, A., Zhang, Y., Wang, W., and Hofzumahaus, A.: Atmospheric OH reactivities in the Pearl River Delta – China in summer 2006: measurement and model results, Atmos. Chem. Phys., 10, 11243–11260, doi:10.5194/acp-10-11243-2010, 2010.
Martinez, M., Harder, H., Kovacs, T. A., Simpas, J. B., Bassis, J., Lesher, R., Brune, W. H., Frost, G. J., Williams, E. J., Stroud, C. A., Jobson, B. T., Roberts, J. M., Hall, S. R., Shetter, R. E., Wert, B., Fried, A., Alicke, B., Stutz, J., Young, V. L., White, A. B., and Zamora, R. J.: OH and HO_2 concentrations, sources, and loss rates during the Southern Oxidants Study in Nashville, Tennessee, summer 1999, J. Geophys. Res., 108, 4617, doi:10.1029/2003JD003551, 2003.
Michoud, V., Kukui, A., Camredon, M., Colomb, A., Borbon, A., Miet, K., Aumont, B., Beekmann, M., Durand-Jolibois, R., Perrier, S., Zapf, P., Siour, G., Ait-Helal, W., Locoge, N.,

AMTD
8, 3803–3850, 2015

Sauvage, S., Afif, C., Gros, V., Furger, M., Ancellet, G., and Doussin, J. F.: Radical budget analysis in a suburban European site during the MEGAPOLI summer field campaign, Atmos. Chem. Phys., 12, 11951–11974, doi:10.5194/acp-12-11951-2012, 2012.

Nölscher, A. C., Williams, J., Sinha, V., Custer, T., Song, W., Johnson, A. M., Axinte, R., Bozem, H., Fischer, H., Pouvesle, N., Phillips, G., Crowley, J. N., Rantala, P., Rinne, J., Kulmala, M., Gonzales, D., Valverde-Canossa, J., Vogel, A., Hoffmann, T., Ouwersloot, H. G., Vilà-Guerau de Arellano, J., and Lelieveld, J.: Summertime total OH reactivity measurements from boreal forest during HUMPPA-COPEC 2010, Atmos. Chem. Phys., 12, 8257–8270, doi:10.5194/acp-12-8257-2012, 2012a.

Nölscher, A. C., Sinha, V., Bockisch, S., Klüpfel, T., and Williams, J.: Total OH reactivity measurements using a new fast Gas Chromatographic Photo-Ionization Detector (GC-PID), Atmos. Meas. Tech., 5, 2981–2992, doi:10.5194/amt-5-2981-2012, 2012b.

Nölscher, A. C., Bourtsoukidis, E., Bonn, B., Kesselmeier, J., Lelieveld, J., and Williams, J.: Seasonal measurements of total OH reactivity emission rates from Norway spruce in 2011, Biogeosciences, 10, 4241–4257, doi:10.5194/bg-10-4241-2013, 2013.

Nölscher, A. C., Butler, T., Auld, J., Veres, P., Munoz, A., Taraborrelli, D., Vereecken, L., Lelieveld, J., and Williams, J.: Using total OH reactivity to assess isoprene photooxidation via measurement and model, Atmos. Environ., 89, 453–463, 2014.

Saunders, S. M., Jenkin, M. E., Derwent, R. G., and Pilling, M. J.: Protocol for the development of the Master Chemical Mechanism, MCM v3 (Part A): tropospheric degradation of non-aromatic volatile organic compounds, Atmos. Chem. Phys., 3, 161–180, doi:10.5194/acp-3-161-2003, 2003.

Sinha, V., Williams, J., Crowley, J. N., and Lelieveld, J.: The Comparative Reactivity Method – a new tool to measure total OH Reactivity in ambient air, Atmos. Chem. Phys., 8, 2213–2227, doi:10.5194/acp-8-2213-2008, 2008.

Sinha, V., Williams, J., Lelieveld, J., Ruuskanen, T. M., Kajos, M. K., Patokoski, J., Hellen, H., Hakola, H., Mogensen, D., Boy, M., Rinne, J., and Kulmala, M.: OH reactivity measurements within a boreal forest: evidence for unknown reactive emissions, Environ. Sci. Technol., 44, 6614–6620, doi:10.1021/es101780b, 2010.

Sinha, V., Williams, J., Diesch, J. M., Drewnick, F., Martinez, M., Harder, H., Regelin, E., Kubistin, D., Bozem, H., Hosaynali-Beygi, Z., Fischer, H., Andrés-Hernández, M. D., Kartal, D., Adame, J. A., and Lelieveld, J.: Constraints on instantaneous ozone production rates and

AMTD
8, 3803–3850, 2015

regimes during DOMINO derived using in-situ OH reactivity measurements, Atmos. Chem. Phys., 12, 7269–7283, doi:10.5194/acp-12-7269-2012, 2012.

Stone, D., Whalley, L. K., and Heard, D. E.: Tropospheric OH and HO_2 radicals: field measurements and model comparisons, Chem. Soc. Rev., 41, 6348–6404, 2012.

Whalley, L. K., Edwards, P. M., Furneaux, K. L., Goddard, A., Ingham, T., Evans, M. J., Stone, D., Hopkins, J. R., Jones, C. E., Karunaharan, A., Lee, J. D., Lewis, A. C., Monks, P. S., Moller, S. J., and Heard, D. E.: Quantifying the magnitude of a missing hydroxyl radical source in a tropical rainforest, Atmos. Chem. Phys., 11, 7223–7233, doi:10.5194/acp-11-7223-2011, 2011.

Zannoni, N., Dusanter, S., Gros, V., Sarda Esteve, R., Michoud, V., Sinha, V., Locoge, N., Bonsang, B., Intercomparison of two comparative reactivity method instruments in the Mediterranean basin during summer 2013, Atmos. Meas. Tech. Discuss., in preparation, 2015.

AMTD
8, 3803–3850, 2015

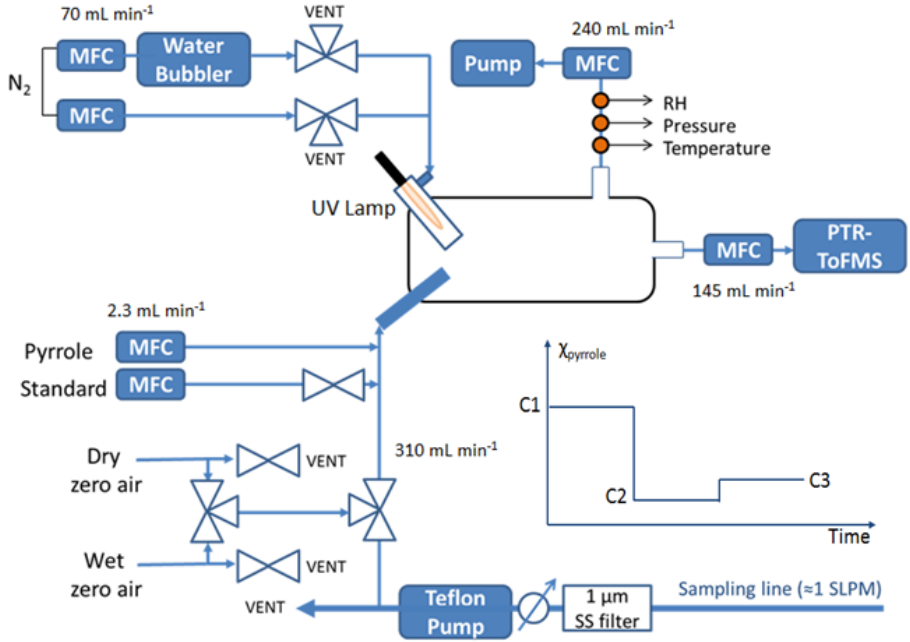

Figure 1. Schematic of the Comparative Reactivity Method instrument developed at Mines Douai. The flow rates of different gases injected inside the CRM reactor are shown (Pyrrole, N_2, PTR-MS sampling, reactor exhaust, air sampling). The insert displays the pyrrole mixing ratios (C1, C2, C3) monitored during OH reactivity measurements.

AMTD
8, 3803–3850, 2015

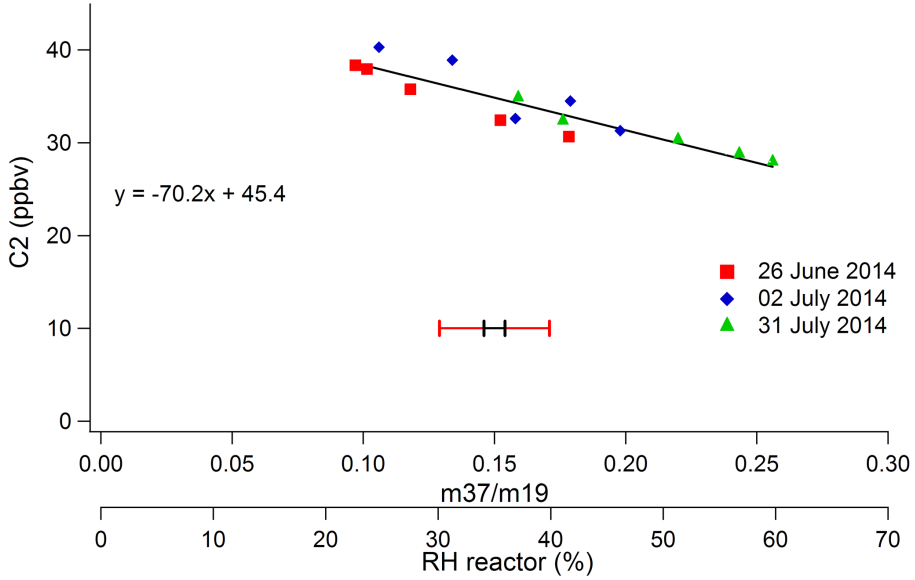

Figure 2. Changes in C2 due to changes in RH. RH is tracked using the m37/m19 ratio monitored by PTR-MS (the corresponding RH measured in the reactor at 22 °C is given on a second axis). Three experiments conducted during the Dunkirk 2014 field campaign are presented. The solid black line represents a linear regression for the three experiments. Black and red intervals are the mean and the maximum variations of m37/m19 observed between C2 and C3 during the Dunkirk campaign, respectively.

AMTD
8, 3803–3850, 2015

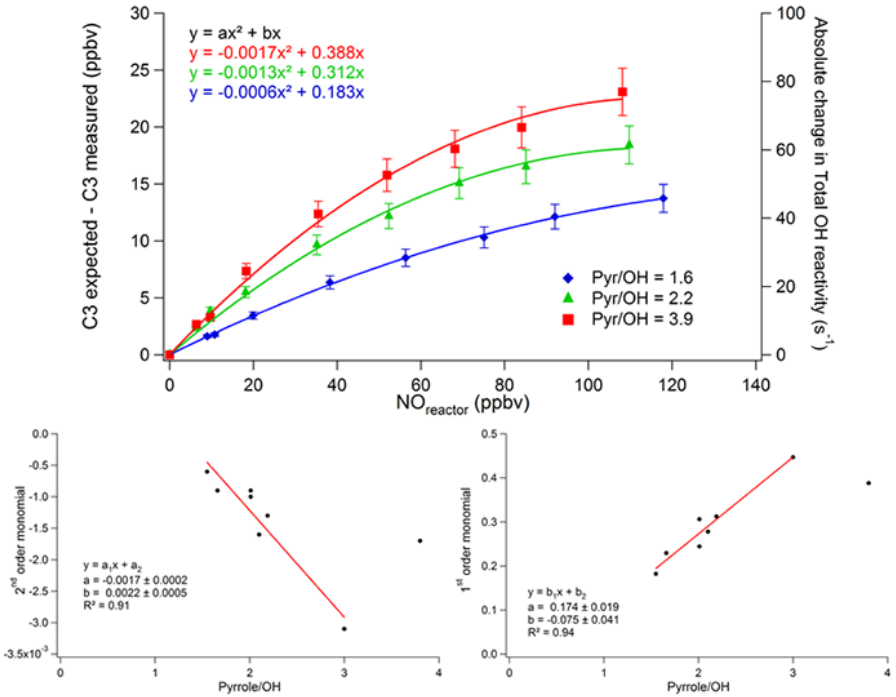

Figure 3. Experimental parameterization to correct for the NO interference. Top panel: changes in C3 (ΔC3 = C3 expected – C3 measured, left axis) as a function of NO mixing ratios in the reactor. Three experiments conducted at Pyrrole-to-OH ratios of 1.6 (blue diamonds), 2.2 (green triangles) and 3.9 (red squares) are shown. The right axis corresponds to the absolute change in total OH reactivity for the experiment conducted at a pyrrole-to-OH ratio of 2.2. Solid lines are quadratic regressions, which equations are shown. Error bars are uncertainties on ΔC3 (approximately 9 %) calculated by a quadratic propagation of errors. Bottom panel: trends of the 1st (right) and 2nd (left) order monomials with the pyrrole-to-OH ratio for the quadratic regressions presented in top panel. Results of the experiment performed using dry zero air (Pyrrole-to-OH ratio of 3.9) is not taken into account in the linear fits (see text).

AMTD
8, 3803–3850, 2015

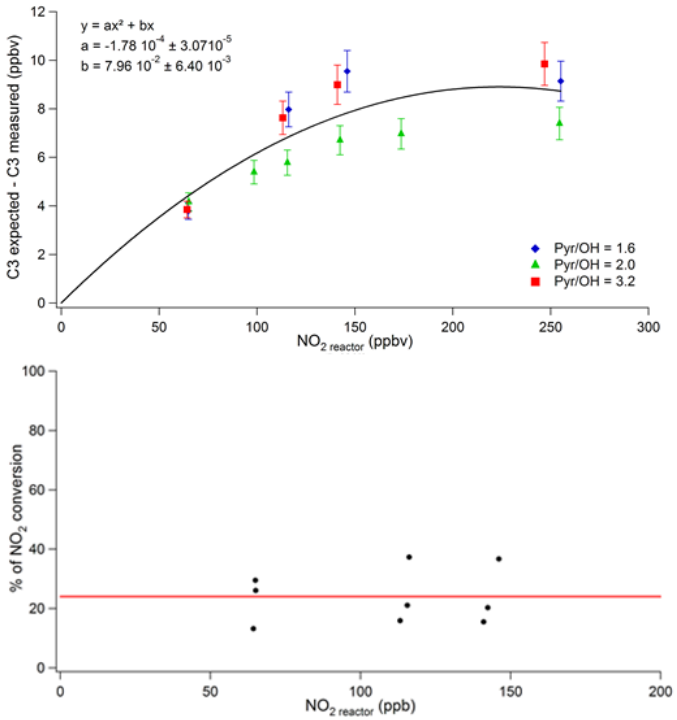

Figure 4. Experimental parameterization to correct for the NO_2 interference. Top panel: changes in C3 (ΔC3 = C3 expected – C3 measured) as a function of NO_2 mixing ratios in the reactor. Three experiments conducted at Pyrrole-to-OH ratios of 1.6 (blue diamonds), 2.0 (green triangles), and 3.2 (red squares) are shown. Error bars are uncertainties on ΔC3 (approximately 9 %) calculated by a quadratic propagation of errors. The black line and the equation correspond to the quadratic regression for the three experiments. Bottom panel: quantification of the NO_2 fraction converted into NO (see text). The red line is the mean value (≈ 24 %) derived for NO_2 conversion.

AMTD
8, 3803–3850, 2015

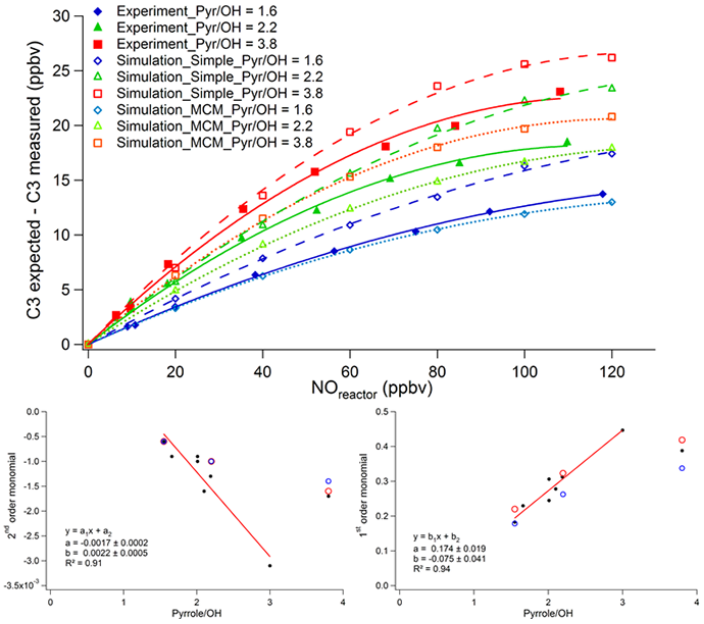

Figure 5. Comparison of laboratory observations to model simulations for the NO interference. Top panel: experimental (filled symbols and solid lines) and simulated (open symbols and dashed (Simple Mechanism) or dotted (MCM) lines) results. The changes in C3 (ΔC3 = C3 expected – C3 measured) is shown as a function of NO mixing ratios in the reactor. Experimental values are the same than in Fig. 3. Simulated values are from the use of the two mechanisms described in Sect. 3 (the simple mechanism and the MCM) at the same Pyrrole-to-OH ratios than the experiments (same color code) and under dry conditions. Bottom panel: experimental (black dots) and simulated (red open circles and blue open circles for the simple mechanism and MCM, respectively) showing the trends of the 1st (right) and 2nd (left) order monomials with the pyrrole-to-OH ratio for the quadratic regressions presented in the top panel. The red lines and the equations correspond to linear regressions adjusted on the experimental results not considering experiment using dry zero air (Pyrrole-to-OH ratio of 3.9, see text).

AMTD
8, 3803–3850, 2015

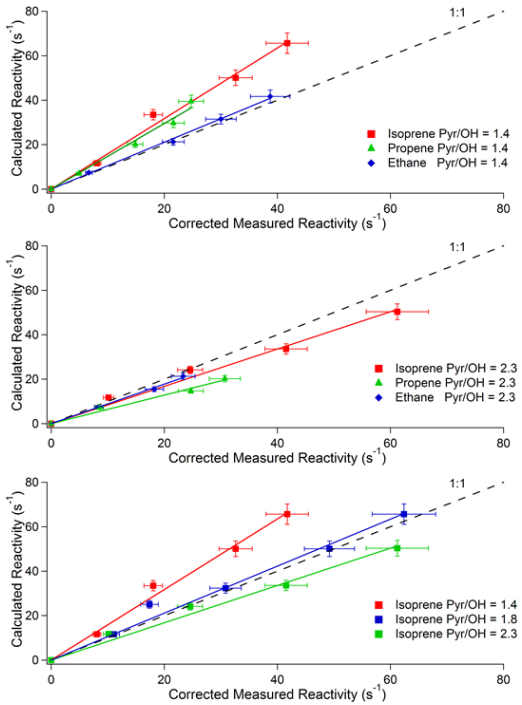

Figure 6. Experimental investigations of the bias caused by a deviation from pseudo first-order kinetics. Comparison of calculated reactivity (true reactivity) to measured reactivity during standard additions into the reactor. Top panel: results from the addition of three different standards (Isoprene: red squares, Ethane: blue diamonds and Propene: green triangles), characterized by different reaction rate constants with OH (1.0×10^{-10}, 2.4×10^{-13}, 2.9×10^{-11} cm^3 $molecules^{-1}$ s^{-1}, respectively), at a pyrrole-to-OH ratio of 1.4. Middle panel: results from the addition of the three standards at a pyrrole-to-OH ratio of 2.3. Bottom panel: results from the addition of the isoprene standard at three different pyrrole-to-OH ratios (1.4: red squares, 1.8: blue squares, 2.3: green squares).

AMTD
8, 3803–3850, 2015

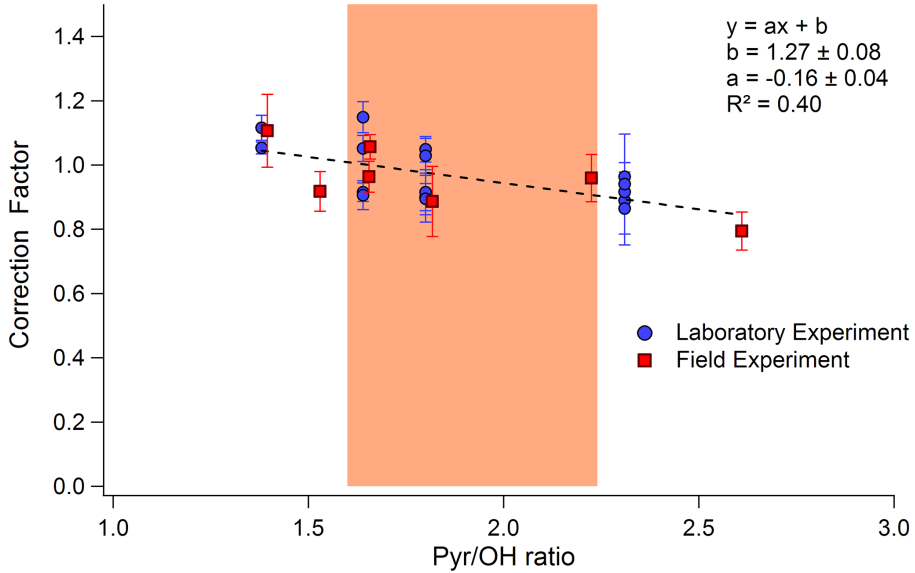

Figure 7. Trend of the correction factor with the pyrrole-to-OH ratio. The correction factors represent the slopes of scatter plots (as shown in Fig. 6) during different laboratory (blue circles) and field (red squares) experiments over a period of 7 months. Error bars are the 1σ uncertainties of the slopes determined for each experiment. The colored area is the range of Pyrrole-to-OH ratios generally observed in the field (1.6–2.2) for the MD-CRM instrument.

AMTD
8, 3803–3850, 2015

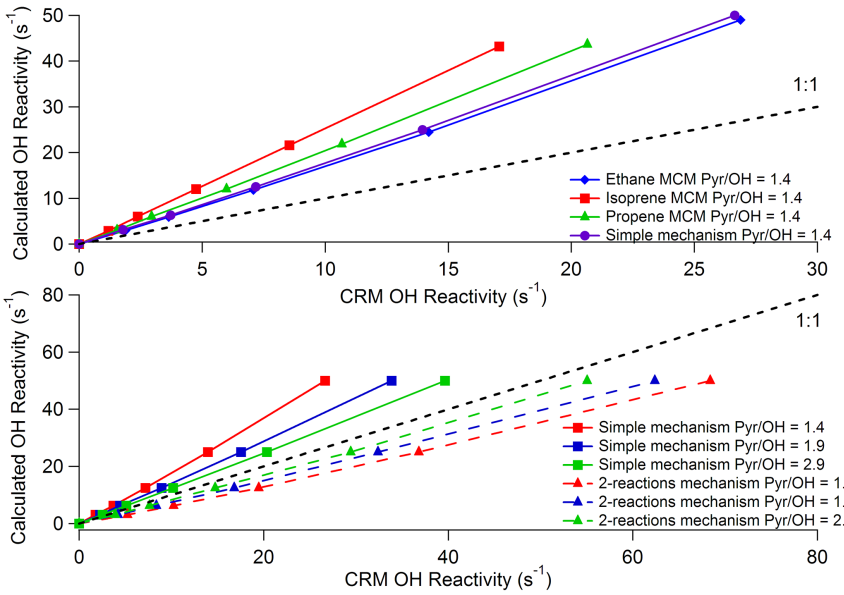

Figure 8. Simulations of the bias caused by a deviation from pseudo first-order kinetics. Comparison of calculated (real OH reactivity) to simulated (simulation of the C1-C2-C3 modulations) OH reactivity values from standard addition in the model. Top panel: results from the addition of four different standards (Isoprene: red squares, Ethane: blue diamonds and Propene: green triangles, and a surrogate standard from the simple mechanism: purple circles), characterized by different reaction rate constants with OH (1.0×10^{-10}, 2.4×10^{-13}, 2.9×10^{-11}, 5.0×10^{-12} cm^3 $molecules^{-1}$ s^{-1} respectively), at a pyrrole-to-OH ratio of 1.4. Simulations were conducted using the MCM and the simple mechanism as indicated in the legend. Bottom panel: results from the addition of a unique standard at three different pyrrole-to-OH ratios (1.4: red symbols, 1.9: blue symbols, 2.9: green symbols) for simulations conducted with the simple mechanism (squares) and the 2-reaction mechanism (see text, triangles). The gas standard added in the model for the two mechanisms has a reaction rate constant toward OH of 5.0×10^{-12} cm^3 $molecules^{-1}$ s^{-1}.

AMTD
8, 3803–3850, 2015

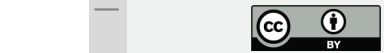

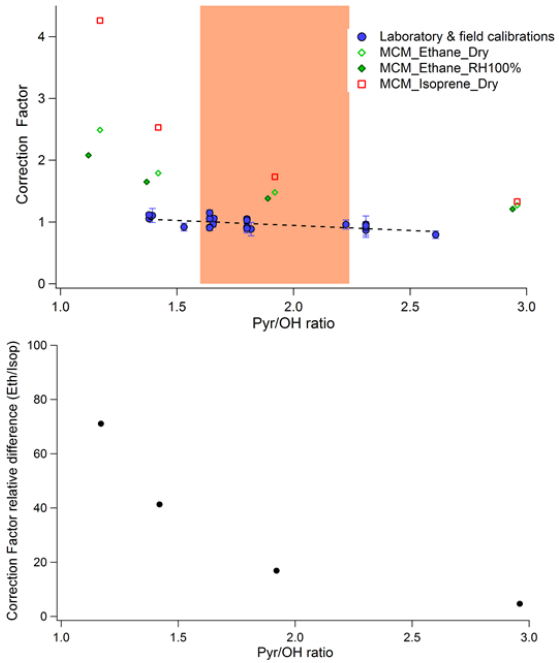

Figure 9. Comparison of correction factors derived for a deviation from pseudo first order kinetics from laboratory observations and model simulations. Top panel: trends of the simulated and measured correction factors with the pyrrole-to-OH ratio. The measured correction factors (blues circles) are the same than in Fig. 7. The simulated correction factors stem from simulations conducted using the model including MCM and constrained with ethane under dry conditions (green open diamonds) and wet conditions (green filled diamonds), or with isoprene under dry conditions (red open squares). The colored area corresponds to the range of Pyrrole-to-OH ratios generally observed in the field (1.6–2.2) for the MD-CRM instrument. Bottom panel: trend of the relative difference between correction factors simulated under dry conditions for ethane and isoprene as a function of the pyrrole-to-OH ratio. Relative difference calculated as $100 \times (F_{\text{isoprene}} - F_{\text{ethane}})/F_{\text{ethane}}$.

AMTD
8, 3803–3850, 2015

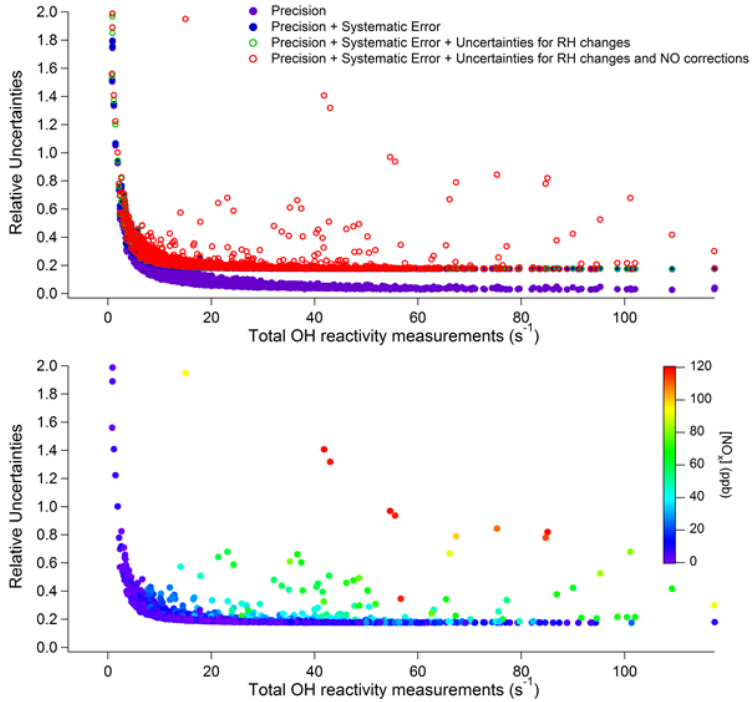

Figure 10. Total OH reactivity measurements uncertainties calculated for the Dunkirk field campaign during July 2014. Top panel: precision and relative uncertainties as a function of total OH reactivity measurements. Different levels of uncertainties are considered: the precision observed when measuring the pyrrole signal (purple dots), the total uncertainty based on a propagation of the measurement precision and systematic errors, except for the humidity and NO corrections (blue dots), the total uncertainty accounting for the precision, systematic errors, and both the humidity (green open dots) and the humidity and NO (red open dots) corrections. Bottom panel: overall total uncertainty as a function of total OH reactivity measurements. These data have been color-coded as a function of NO_x levels.

AMTD
8, 3803–3850, 2015

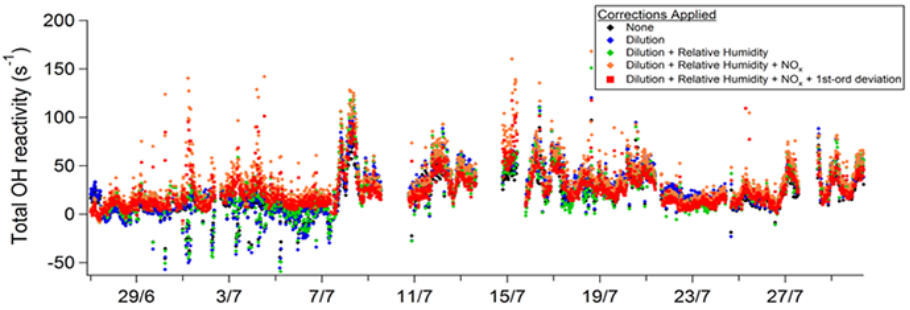

Figure 11. Time series of ambient OH reactivity measurements from MD-CRM during the Dunkirk field campaign, including uncorrected measurements (black symbols), measurements corrected for dilution (blue symbols), measurements corrected for dilution and differences in relative humidity between C2 and C3 (green symbols), measurements corrected for dilution, differences in relative humidity and NO interference (orange symbols), and measurements with all corrections applied (red symbols). These data are preliminary.

AMTD
8, 3803–3850, 2015